MATERIALS CHEMISTRY FRONTIERS

RESEARCH ARTICLE

View Article Online
View Journal | View Issue

Cite this: *Mater. Chem. Front.*, 2020, **4**, 2971

Hollow multishelled structural NiO as a "shelter" for high-performance Li–S batteries†

Yujing Zhu,‡[abc] Jiangyan Wang,‡[b] Chuan Xie,[c] Mei Yang,[b] Zijian Zheng *[c] and Ranbo Yu *[ad]

Received 22nd July 2020,
Accepted 16th August 2020

DOI: 10.1039/d0qm00492h

rsc.li/frontiers-materials

The physical multiple confinement and chemical adsorption of polysulfides are realized with an interlayer composed of non-polar materials (acetylene black) and polar materials (NiO hollow multishelled structures, NiO HoMSs). The 4S-NiO HoMSs/CC-S electrodes show the highest sulfur utilizations, which are 71.64% at 0.2C and 65.86% at 1.0C. The discharge capacity is 860.4 mA h g^{-1} after 200 cycles, with a 73.94% capacity retention rate.

Li–S batteries with unique multi-electron, multi-phase, multi-stage reaction characteristics possess an ultra-high theoretical energy density.[1] However, the practical application of Li–S batteries is limited by several challenges including the volume expansion of sulfur, the intrinsic insulating lithium sulfide,[2] and the shuttle effect of soluble lithium polysulfides (Li_2S_n, $4 \leqslant n \leqslant 8$, LiPSs),[3] which result in a low utilization of active materials and Coulombic efficiency, rapid capacity decay and poor practically-achievable energy density.[4] To address these problems, tremendous efforts have been devoted to constructing sulfur hosts and battery configurations, for instance from the initial non-polar mesoporous carbon materials[5] to the heteroatom-doped carbon materials,[6,7] and metal compounds,[8–10] as well as the functionalization of separators[11,12] and interlayers.[13–15] Polar compounds possess a stronger ability to entrap LiPSs in the cathode.[16] As important as the material components is the geometry. Hollow nanostructured sulfur hosts have been reported to physicochemically control LiPS diffusion, as well as to increase the sulfur loading and accommodate the volume expansion.[17–26] Wang's group synthesized a TiO_{2-x} hollow multishelled structure (HoMS) as the sulfur host.[25] The unique multishelled structures achieved multi-stage confinement of soluble LiPSs, thus obtaining a long cycle life. Hollow multishelled structural materials have abundant advantages: (1) the large specific surface area of HoMSs provides more active sites to catalyze the conversion of polysulfides and anchor polysulfides by chemisorption; (2) besides sulfur hosts, the interlayer structure also has become an effective strategy to immobilize polysulfides. Manthiram A.'s group introduced a new strategy on cell configuration instead of sulfur hosts for improving the performance of Li–S batteries.[15] By adding carbon paper as a bifunctional interlayer between the cathode and separator, the active material utilization and polysulfide reutilization have been greatly facilitated. Afterwards, interlayer materials such as carbon (carbon nanotube (CNT),[27] graphene[28]), metal oxides (V_2O_5,[14] MnO_2[29]), Ti_3C_2,[30] and metal sulfides (MoS_2,[31] WS_2[32]) have received extensive attention.

In recent years, the rapid development of flexible and wearable electronic devices has motivated people to develop flexible Li–S batteries.[33–35] The flexibility of sulfur hosts plays a decisive role in flexible Li–S batteries. During the mechanical deformation such as bending, folding and stretching, each component of the flexible electrode should be stably connected in its original position to ensure continuous electron and ion transport. Compared with intrinsically flexible low-dimensional carbon nanomaterials (CNT, carbon nanofiber (CNF)), the commercial carbon cloth (CC) costs less and has a wide availability and stable quality, and thus has been considered as a promising flexible host with a good electrical conductivity and mechanical strength. CC modified with heteroatom-doping[36,37] and *in situ* growth of polar materials[34,38] has been introduced to prepare binder-free cathodes with the enlargement of the surface area and strong chemical adsorption of LiPSs. However, these approaches depended on complex processes. Liu's group developed a non-encapsulation method to load

[a] *Department of Physical Chemistry, School of Metallurgical and Ecological Engineering, University of Science and Technology Beijing, No. 30, Xueyuan Road, Haidian District, Beijing 100083, P. R. China. E-mail: ranboyu@ustb.edu.cn*
[b] *State Key Laboratory of Biochemical Engineering, Institute of Process Engineering, Chinese Academy of Sciences, 1 North 2nd Street, Zhongguancun, Beijing 100190, P. R. China*
[c] *Laboratory for Advanced Interfacial Materials and Devices, Research Center for Smart Wearable Technology, Institute of Textiles and Clothing, The Hong Kong Polytechnic University, Hong Kong, SAR, China. E-mail: tczzheng@polyu.edu.hk*
[d] *Key Laboratory of Advanced Material Processing & Mold (Ministry of Education), Zhengzhou University, Zhengzhou, 450002, P. R. China*

† Electronic supplementary information (ESI) available: Experimental details, SEM, XRD, and TEM images. See DOI: 10.1039/d0qm00492h

‡ These authors contributed equally.

sulfur on carbon fiber with a low-surface-area and realized a high energy density (1835 W h kg^{-1}).[39]

Here, we deposit the active material on the surface of CC through electrochemical deposition to prepare the non-encapsulated sulfur cathode, and used the interlayer structure with acetylene black (AB) and NiO HoMSs to control the LiPS diffusion and improve the sulfur utilization. The effects of non-polar and polar materials as interlayers on electrochemical properties were studied. CC was used as the flexible current collector and sulfur host simultaneously. Single-, double-, triple- and quadruple-shelled NiO hollow sphere (denoted as NiO hollow spheres, 2S-NiO HoMSs, 3S-NiO HoMSs, 4S-NiO HoMSs) materials were synthesized by a sequential templating approach,[40–43] and its multishelled structure serves as a temporary "shelter" for LiPSs, providing abundant active sites and preventing LiPSs from diffusing to the anode electrode, thus achieving a high sulfur utilization. The first discharge capacity of the 4S-NiO/CC-S electrode was 1169.9 mA h g^{-1} at 0.2C and the discharge capacity maintained at 960.6 mA h g^{-1} after 100 cycles at 1.0C (1.0C = 1675.0 mA g^{-1}).

Fig. 1 shows the structure of the Li–S battery. The cathode electrode is CC, with an interlayer between the separator and the cathode electrode. The CC performs multiple functions of electrode flexibility, cathode current collector, and reaction sites for active materials and polysulfides. Fig. S1 and S2 (ESI†) show the TEM and XRD of the prepared NiO HoMSs. Li_2S_8 could be dispersed evenly on the surface of CC by dropping (Fig. S4, ESI†). The morphological images of the active material on the surface of the carbon fiber after the first discharge process at 0.1C are observed in Fig. 2a–c. After the discharge process, the gap between the carbon fibers was filled with active materials, and Li_2S nanosheets were observed on the surface of carbon fibers. The open nanosheet structure is considered to be beneficial to electron and ion transport, increasing the specific capacity of the active material and reducing the overpotential.[39] The filling of interstitial spaces between the fibers also contributes to the increase in volumetric energy density. However, after repeating charge/discharge processes several times, nanosheets disappeared to irregularly shaped Li_2S nanoparticles (Fig. 2d–f), which can be attributed to the following two reasons. Firstly, sulfur species are prone to grow where sulfur is present, rather than growing evenly along the surface of the carbon fiber.[39] Secondly, the dissolution of intermediate

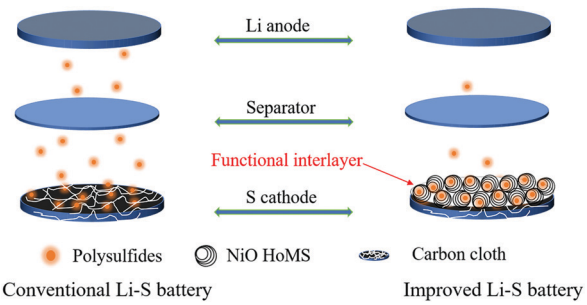

Fig. 1 The structure of the Li–S battery.

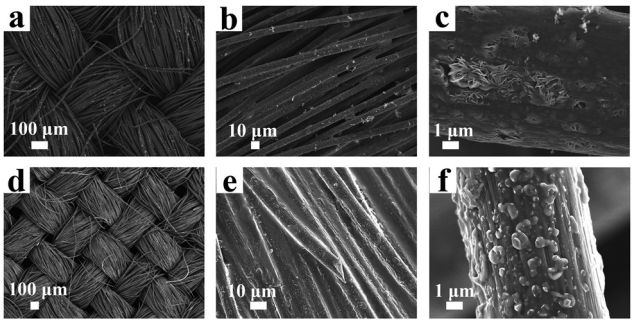

Fig. 2 SEM images of active materials on the surface of the carbon fiber. (a)–(c) After the first discharge process, and (d and e) after repeated charge/discharge processes for 5 cycles.

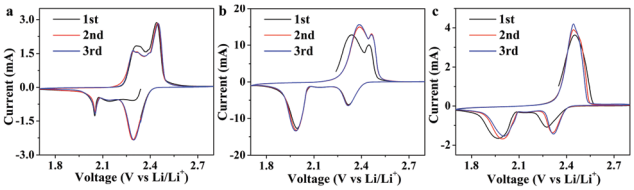

Fig. 3 Cyclic voltammetry (CV) curves of different electrodes: (a) CC-S electrodes; (b) AB/CC-S electrode; and (c) the NiO HoMSs/CC-S electrode at 0.2 mV s^{-1}.

polysulfides gives rise to the random precipitation of Li_2S all over the electrode upon discharge.[44]

CV curves of three different electrodes (bare CC-S electrode, CC-S electrodes covered by AB interlayer defined as AB/CC-S electrode, CC-S electrodes covered by the mixture of NiO HoMSs with AB interlayer defined as NiO HoMSs/CC-S electrode) are evaluated before the electrochemical measurement in the voltage window of 1.7–2.8 V in Fig. 3. Two reduction peaks appeared, wherein the one at high potential corresponds to the reduction of sulfur to soluble long-chain LiPSs, while the one at low potential corresponds to the reduction of long-chain LiPSs to short-chain lithium sulfide and insoluble solid Li_2S_2 and Li_2S. The oxidation peak corresponds to the transformation of solid Li_2S_2 and Li_2S to sulfur. Besides the first cycle, the curves of the second and third cycles coincided well, which indicates the good reversibility of the redox reaction. In the CV curves of the CC-S electrode (Fig. 3a), the intensity of the reduction peak at high potential was significantly greater than that at low potential, which manifests that the capacity contribution from the reduction of sulfur to soluble long-chain LiPSs accounts for a larger proportion in the discharge process, while the shuttle effect of soluble polysulfides will lead to a decrease in the sulfur utilization, resulting in a much smaller capacity of the CC-S electrode. The reduction peak intensity of the AB/CC-S and NiO HoMSs/CC-S electrodes (Fig. 3b and c), at low potential was higher than that at high potential, which makes it clear that the energy contributed by long-chain LiPS reduction to short-chain lithium sulfide and active materials accounts for the major part.

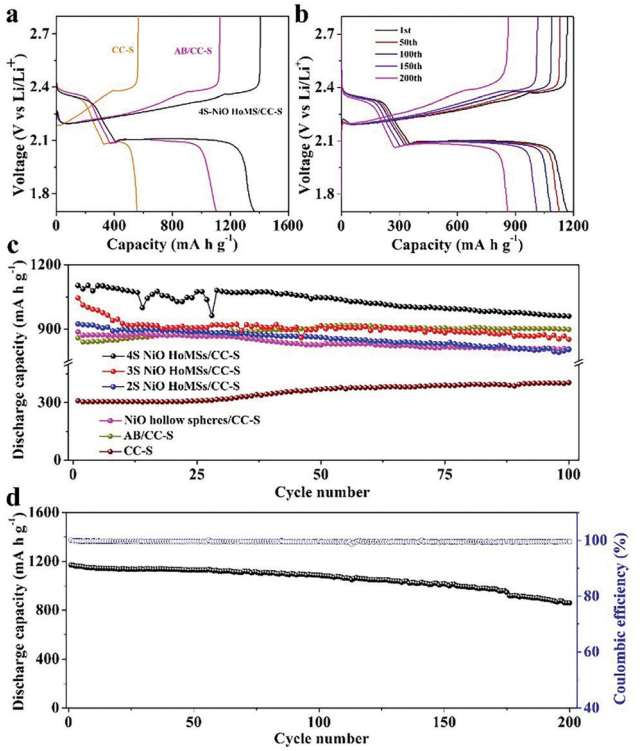

Fig. 4 (a) The first cycle charge/discharge profiles of the CC-S electrode, AB/CC-S electrode and 4S-NiO HoMSs/CC-S electrode at 0.1C. (b) The charge–discharge curves of the 4S-NiO HoMSs/CC-S electrode at 0.2C. (c) Long-cycle stability of different electrodes at 1.0C. (d) Long-cycle stability of the 4S-NiO HoMSs/CC-S electrode at 0.2C.

The first charge and discharge profiles are demonstrated in Fig. 4a. The voltage platform of the charge/discharge curves was consistent with the CV peaks. In the discharge curve, the capacity contribution of the CC-S electrode at low potential platform (*i.e.*, reduction from soluble Li_2S_4 to insoluble Li_2S) was less than 75% of the theoretical value. This is mainly due to the incomplete reduction of LiPSs. The surface of CC is composed of a uniform microporous structure. Polysulfide is reduced to solid insoluble Li_2S, which causes pore blockage and forms a passivation layer on the surface of carbon fiber, thus not only limiting the diffusion of Li^+, but also delaying the reduction of PS in the pore structure which may cause polysulfides to shuttle to the negative electrode.[2] In the AB/CC-S electrode, the acetylene black interlayer could physically limit the shuttle effect of LiPSs, leading to improved sulfur utilization. In the NiO HoMSs/CC-S electrode, in addition to the physical-confinement of LiPSs by the acetylene black, the NiO HoMSs could not only chemically anchor polysulfides but also physically confine LiPS diffusion with favorable multishelled structures, thus significantly improving sulfur utilization and specific capacity.

Fig. 4c shows the cycle stability at a current density of 1.0C. Among all the electrodes, the 4S NiO HoMSs/CC-S electrode exhibits the best performance, achieving the largest sulfur utilization ratio of 65.86%, and the highest initial discharge capacity of 1103.2 mA h g^{-1} which maintained 960.6 mA h g^{-1} after 100 cycles. The first discharge capacities of 3S-NiO HoMSs/CC-S, 2S-NiO HoMSs/CC-S and NiO hollow spheres/CC-S electrodes were 1045.3, 923.5 and 886.4 mA h g^{-1}, respectively. And the discharge capacities after 100 cycles were 851.6, 803.7 and 806.0 mA h g^{-1}, respectively. The change trend could be more clearly understood from the histogram (Fig. S5, ESI†): the capacity of the electrode increased as the number of NiO shells increased. This is mainly because with the increase of shell number, the active sites for chemical adsorption and catalysis of the polysulfides also increases. The pore structure on the shell allows the polysulfides to enter the interior of the hollow spheres, and the physical confinement effect was also enhanced. The first discharge capacities of the AB/CC-S electrodes and CC-S electrodes were 858.1 and 309.2 mA h g^{-1}, respectively, corresponding to a sulfur utilization of 51.23% and 18.46%, respectively. The discharge capacities slightly increased to 898.1 and 404.3 mA h g^{-1}, respectively, after 100 cycles.

Fig. 4d shows the charge/discharge curves and long-cycling stability of the 4S-NiO HoMSs/CC-S electrode at 0.2C. The 4S electrode maintained a long and stable voltage platform even after 200 cycles. The first discharge capacity and sulfur utilization were 1169.9 mA h g^{-1} and 71.64%, respectively. After 200 cycles, the discharge capacity was 860.4 mA h g^{-1}, and the capacity retention rate was 73.94%, demonstrating a good cycling stability.

Conclusions

In summary, a fabric-based interlayer with NiO HoMSs for Li–S batteries was constructed. The multifunctional interlayer architecture effectively improves the utilization efficiency of sulfur, the specific capacity and cycling stability, by realizing both the physiochemical adsorption and the multi-stage physical confinement of soluble polysulfides. The 4S-NiO HoMSs/CC-S electrode achieved the highest discharge capacity, showing a sulfur utilization efficiency nearly four times that of the CC-S electrode. In addition, it was found that as the shell number increased, the active sites for chemical adsorption and catalysis of the polysulfide also increased, and the physical confinement effect also improved. This demonstrates that polar NiO hollow multishelled structural materials are very powerful in improving the utilization efficiency of sulfur and limiting the shuttling of polysulfides.

Conflicts of interest

There are no conflicts to declare.

Acknowledgements

This work was financially supported by NSFC/RGC Joint Research Scheme (N_PolyU528/16) and National Natural Science Foundation of China (No. 51661165013, 51872024, 21671016, 51932001, 21590795, 21821005, and 21820102002).

References

1 P. G. Bruce, S. A. Freunberger, L. J. Hardwick and J. M. Tarascon, Li–O_2 and Li–S batteries with high energy storage, *Nat. Mater.*, 2011, **11**, 19–29.

2 H. Chu, H. Noh, Y. J. Kim, S. Yuk, J. H. Lee, J. Lee, H. Kwack, Y. Kim, D. K. Yang and H. T. Kim, Achieving three-dimensional lithium sulfide growth in lithium–sulfur batteries using high-donor-number anions, *Nat. Commun.*, 2019, **10**, 188.

3 Y. V. Mikhaylik and J. R. Akridge, Polysulfide shuttle study in the Li/S battery system, *J. Electrochem. Soc.*, 2004, **151**, A1969.

4 J. Wang, Y. Cui and D. Wang, Design of hollow nanostructures for energy storage, conversion and production, *Adv. Mater.*, 2019, **31**, 1801993.

5 X. Ji, K. T. Lee and L. F. Nazar, A highly ordered nanostructured carbon–sulphur cathode for lithium–sulphur batteries, *Nat. Mater.*, 2009, **8**, 500–506.

6 Y. Dong and T. Ben, Impregnated sulfur in carbonized nitrogen-containing porous organic frameworks as cathode with high rate performance and long cycle life for lithium–sulfur batteries, *Chem. Res. Chin. Univ.*, 2019, **35**, 654–661.

7 T. Z. Hou, X. Chen, H. J. Peng, J. Q. Huang, B. Q. Li, Q. Zhang and B. Li, Design principles for heteroatom-doped nanocarbon to achieve strong anchoring of polysulfides for lithium–sulfur batteries, *Small*, 2016, **12**, 3283–3291.

8 X. Liang, C. Hart, Q. Pang, A. Garsuch, T. Weiss and L. F. Nazar, A highly efficient polysulfide mediator for lithium–sulfur batteries, *Nat. Commun.*, 2015, **6**, 5682.

9 J. Balach, J. Linnemann, T. Jaumann and L. Giebeler, Metal-based nanostructured materials for advanced lithium–sulfur batteries, *J. Mater. Chem. A*, 2018, **6**, 23127–23168.

10 X. Liu, J. Q. Huang, Q. Zhang and L. Mai, Nanostructured metal Oxides and sulfides for lithium–sulfur batteries, *Adv. Mater.*, 2017, **29**, 1601759.

11 S. Bai, X. Liu, K. Zhu, S. Wu and H. Zhou, Metal–organic framework-based separator for lithium–sulfur batteries, *Nat. Energy*, 2016, **1**, 16094.

12 Z. A. Ghazi, X. He, A. M. Khattak, N. A. Khan, B. Liang, A. Iqbal, J. Wang, H. Sin, L. Li and Z. Tang, MoS_2/Celgard separator as efficient polysulfide barrier for long-life lithium–sulfur batteries, *Adv. Mater.*, 2017, **29**, 1606817.

13 J.-L. Qin, B.-Q. Li, J.-Q. Huang, L. Kong, X. Chen, H.-J. Peng, J. Xie, R. Liu and Q. Zhang, Graphene-based Fe-coordinated framework porphyrin as an interlayer for lithium–sulfur batteries, *Mater. Chem. Front.*, 2019, **3**, 615–619.

14 Y. Guo, Y. Zhang, Y. Zhang, M. Xiang, H. Wu, H. Liu and S. Dou, Interwoven V_2O_5 nanowire/graphene nanoscroll hybrid assembled as efficient polysulfide-trapping-conversion interlayer for long-life lithium–sulfur batteries, *J. Mater. Chem. A*, 2018, **6**, 19358–19370.

15 Y. S. Su and A. Manthiram, Lithium–sulphur batteries with a microporous carbon paper as a bifunctional interlayer, *Nat. Commun.*, 2012, **3**, 1166.

16 Q. Pang, D. Kundu, M. Cuisinier and L. F. Nazar, Surface-enhanced redox chemistry of polysulphides on a metallic and polar host for lithium–sulphur batteries, *Nat. Commun.*, 2014, **5**, 4759.

17 J. Wang, B. Zhou, H. Zhao, M. Wu, Y. Yang, X. Sun, D. Wang and Y. Du, A sandwich-type sulfur cathode based on multifunctional ceria hollow spheres for high-performance lithium–sulfur batteries, *Mater. Chem. Front.*, 2019, **3**, 1317–1322.

18 N. Jayaprakash, J. Shen, S. S. Moganty, A. Corona and L. A. Archer, Porous hollow carbon@sulfur composites for high-power lithium–sulfur batteries, *Angew. Chem., Int. Ed.*, 2011, **50**, 5904.

19 C. Zhang, H. B. Wu, C. Yuan, Z. Guo and X. W. (David) Lou, Confining sulfur in double-shelled hollow carbon spheres for lithium–sulfur batteries, *Angew. Chem., Int. Ed.*, 2012, **51**, 9592–9595.

20 L. Yu, H. Hu, H. B. Wu and X. W. Lou, Complex hollow nanostructures: synthesis and energy-related applications, *Adv. Mater.*, 2017, **29**, 1604563.

21 Z. Li, J. T. Zhang, Y. M. Chen, J. Li and X. W. Lou, Pie-like electrode design for high-energy density lithium–sulfur batteries, *Nat. Commun.*, 2015, **6**, 8850.

22 Z. Wei Seh, W. Li, J. J. Cha, G. Zheng, Y. Yang, M. T. McDowell, P. C. Hsu and Y. Cui, Sulphur–TiO_2 yolk-shell nanoarchitecture with internal void space for long-cycle lithium–sulphur batteries, *Nat. Commun.*, 2013, **4**, 1331.

23 L. Hu, C. Dai, H. Liu, Y. Li, B. Shen, Y. Chen, S.-J. Bao and M. Xu, Double-shelled NiO–$NiCo_2O_4$ heterostructure@carbon hollow nanocages as an efficient sulfur host for advanced lithium–sulfur batteries, *Adv. Energy Mater.*, 2018, **8**, 1800709.

24 F. Ma, J. Liang, T. Wang, X. Chen, Y. Fan, B. Hultman, H. Xie, J. Han, G. Wu and Q. Li, Efficient entrapment and catalytic conversion of lithium polysulfides on hollow metal oxide submicro-spheres as lithium–sulfur battery cathodes, *Nanoscale*, 2018, **10**, 5634–5641.

25 J. Zhao, M. Yang, N. Yang, J. Wang and D. Wang, Hollow micro-/nanostructure reviving lithium–sulfur batteries, *Chem. Res. Chin. Univ.*, 2020, **36**, 313–319.

26 E. H. M. Salhabi, J. Zhao, J. Wang, M. Yang, B. Wang and D. Wang, Hollow multi-shelled structural TiO_{2-x} with multiple spatial confinement for long-life lithium–sulfur batteries, *Angew. Chem., Int. Ed.*, 2019, **58**, 9078–9082.

27 M. Li, W. Wahyudi, P. Kumar, F. Wu, X. Yang, H. Li, L. J. Li and J. Ming, Scalable approach to construct free-standing and flexible carbon networks for lithium–sulfur battery, *ACS Appl. Mater. Interfaces*, 2017, **9**, 8047–8054.

28 D. K. Lee, S. J. Kim, Y. J. Kim, H. Choi, D. W. Kim, H. J. Jeon, C. W. Ahn, J. W. Lee and H. T. Jung, Graphene oxide/carbon nanotube bilayer flexible membrane for high-performance Li–S batteries with superior physical and electrochemical properties, *Adv. Mater. Interfaces*, 2019, **6**, 1801992.

29 W. Kong, L. Yan, Y. Luo, D. Wang, K. Jiang, Q. Li, S. Fan and J. Wang, Ultrathin MnO_2/graphene oxide/carbon nanotube

interlayer as efficient polysulfide-trapping shield for high-performance Li–S batteries, *Adv. Funct. Mater.*, 2017, **27**, 1606663.

30 Y. Dong, S. Zheng, J. Qin, X. Zhao, H. Shi, X. Wang, J. Chen and Z. S. Wu, All-mXene-based integrated electrode constructed by Ti_3C_2 nanoribbon framework host and nanosheet interlayer for high-energy-density Li–S batteries, *ACS Nano*, 2018, **12**, 2381.

31 L. Tan, X. Li, Z. Wang, H. Guo and J. Wang, Lightweight reduced graphene oxide@MoS_2 interlayer as polysulfide barrier for high-performance lithium–sulfur batteries, *ACS Appl. Mater. Interfaces*, 2018, **10**, 3707.

32 J. Park, B.-C. Yu, J. S. Park, J. W. Choi, C. Kim, Y.-E. Sung and J. B. Goodenough, Tungsten disulfide catalysts supported on a carbon cloth interlayer for high performance Li–S battery, *Adv. Energy Mater.*, 2017, **7**, 1602567.

33 J. Chang, J. Shang, Y. Sun, L. K. Ono, D. Wang, Z. Ma, Q. Huang, D. Chen, G. Liu, Y. Cui, Y. Qi and Z. Zheng, Flexible and stable high-energy lithium–sulfur full batteries with only 100% oversized lithium, *Nat. Commun.*, 2018, **9**, 4480.

34 Z. Wang, J. Shen, J. Liu, X. Xu, Z. Liu, R. Hu, L. Yang, Y. Feng, J. Liu, Z. Shi, L. Ouyang, Y. Yu and M. Zhu, Self-supported and flexible sulfur cathode enabled via synergistic confinement for high-energy-density lithium–sulfur batteries, *Adv. Mater.*, 2019, **31**, 1902228.

35 J. Wang, G. Yang, J. Chen, Y. Liu, Y. Wang, C. Y. Lao, K. Xi, D. Yang, C. J. Harris, W. Yan, S. Ding and R. V. Kumar, Flexible and high-loading lithium–sulfur batteries enabled by integrated three-in-one fibrous membranes, *Adv. Energy Mater.*, 2019, **9**, 1902001.

36 K. Xiao, J. Wang, Z. Chen, Y. Qian, Z. Liu, L. Zhang, X. Chen, J. Liu, X. Fan and Z. X. Shen, Improving polysulfides adsorption and redox kinetics by the Co_4N nanoparticle/N-doped carbon composites for lithium–sulfur batteries, *Small*, 2019, **15**, 1901454.

37 M. Chen, W. Xu, S. Jamil, S. Jiang, C. Huang, X. Wang, Y. Wang, H. Shu, K. Xiang and P. Zeng, Multifunctional heterostructures for polysulfide suppression in high-performance lithium–sulfur cathode, *Small*, 2018, **14**, 1803134.

38 J. Shen, X. Xu, J. Liu, Z. Liu, F. Li, R. Hu, J. Liu, X. Hou, Y. Feng, Y. Yu and M. Zhu, Mechanistic understanding of metal phosphide host for sulfur cathode in high-energy-density lithium–sulfur batteries, *ACS Nano*, 2019, **13**, 8986–8996.

39 H. Pan, J. Chen, R. Cao, V. Murugesan, N. N. Rajput, K. S. Han, K. Persson, L. Estevez, M. H. Engelhard, J.-G. Zhang, K. T. Mueller, Y. Cui, Y. Shao and J. Liu, Non-encapsulation approach for high-performance Li–S batteries through controlled nucleation and growth, *Nat. Energy*, 2017, **2**, 813–820.

40 H. Li, H. Ma, M. Yang, B. Wang, H. Shao, L. Wang, R. Yu and D. Wang, Highly controlled synthesis of multi-shelled NiO hollow microspheres for enhanced lithium storage properties, *Mater. Res. Bull.*, 2017, **87**, 224–229.

41 D. Mao, J. Wan, J. Wang and D. Wang, Sequential Templating Approach: A Groundbreaking Strategy to Create Hollow Multishelled Structures, *Adv. Mater.*, 2019, **31**, 1802874.

42 X. Lai, J. Li, B. A. Korgel, Z. Dong, Z. Li, F. Su, J. Du and D. Wang, General synthesis and gas-sensing properties of multiple-shell metal oxide hollow microspheres, *Angew. Chem., Int. Ed.*, 2011, **50**, 2738–2741.

43 C. Wang, J. Wang, W. Hu and D. Wang, *Chem. Res. Chin. Univ.*, 2020, **36**, 68–73.

44 Z. W. Seh, J. H. Yu, W. Li, P. C. Hsu, H. Wang, Y. Sun, H. Yao, Q. Zhang and Y. Cui, Two-dimensional layered transition metal disulphides for effective encapsulation of high-capacity lithium sulphide cathodes, *Nat. Commun.*, 2014, **5**, 5017.